Hindawi
Advances in Civil Engineering
Volume 2019, Article ID 5347683, 14 pages
https://doi.org/10.1155/2019/5347683

Research Article

Stability Analysis and Monitoring Method for the Key Block Structure of the Basic Roof of Noncoal Pillar Mining with Automatically Formed Gob-Side Entry

Jianning Liu,[1,2] **Manchao He**,[1] **Yajun Wang**,[1,2,3] **Ruifeng Huang**,[1,2] **Jun Yang**,[1,2] **Xichun Tian**,[1,2] **Can Ming**,[1,2] **and Shan Guo**[1,2]

[1]*State Key Laboratory for Geomechanics & Deep Underground Engineering, China University of Mining & Technology (Beijing), Beijing 100083, China*
[2]*School of Mechanics and Civil Engineering, China University of Mining & Technology (Beijing), Beijing 100083, China*
[3]*Department of Geotechnical Engineering, Tongji University, Shanghai 200092, China*

Correspondence should be addressed to Yajun Wang; yyajun1990@163.com

Received 2 July 2019; Revised 27 August 2019; Accepted 11 September 2019; Published 16 October 2019

Academic Editor: Annan Zhou

The key block of the basic roof is the main contributor to the structural stability of a roadway. Research on the stability of the key block structure is of great significance for the promotion of noncoal pillar mining with automatically formed gob-side entry (GEFANM) technology. This paper is set in the engineering context of the GEFANM experiment at the Ningtiaota Coal Mine. The study fully considered the differences in the gob roof caving on the roof-cutting-line side, and the range of rotation angles to maintain a stable key block was determined. Based on this range of rotation angles, the range of safe bulking coefficients of gangue was calculated. The bulking coefficient of the gangue on the gravel side of the roadway was used as the metric in a new monitoring method and in the calculation of the field parameters. The range of safe bulking coefficients was determined to be 1.40–1.37. Field monitoring was conducted to obtain the gangue bulking coefficient on the gravel side. Combining the roof and floor convergence data, when the bulking coefficient fell within the safe range, the convergence was 95–113 mm. In this stage, the key block structure was stable. When the gangue bulking coefficient fell outside the safe range, the convergence was larger, and cracks were observed. The key block may be vulnerable to instability. The results affirmed that the gangue bulking coefficient can be used as a monitoring metric to study the stability of key block structures.

1. Introduction

Coal is a principal energy source, and concerns regarding green and efficient coal mining and the increase in coal mining intensity and depth have drawn considerable attention [1–7]. Traditional longwall mining technology requires two roadways to be constructed in advance with one protective coal pillar retained. However, because of two existing problems, achieving a green and efficient mining process by utilizing longwall mining technology has been substantially constrained. First, the retention of the coal pillars may lead to a serious waste of coal resources in the mining area; second, the tunneling speed may affect the continuation of working face recovery. With respect to coal pillar retention, to optimize the size of the retained pillar and maximize the recovery of coal resources, researchers have investigated the law of stress change and the pillar failure mechanism in the mining area using laboratory experiments, numerical calculations, and on-site monitoring [8–13]. Nonetheless, the problems existing in traditional longwall mining technology cannot be resolved by optimizing the size of the coal pillars, and nonpillar mining technology has become a research focus in the field of coal mining. In some studies of conventional gob-side entry technology, the stability of the roof structure in the roadway was analyzed, the law of underground pressure was determined, and the roadway support parameters were optimized [14–20]. In the practice of conventional gob-side

entry retention, inadequate caving of the gob-side roof results in a thicker hanging roof, and the roadway pressure is high. This technique is difficult to support, and to sustain the stability of the roadway structure, the roadway support cost must be increased. In view of the many problems in conventional gob-side entry retention, the team led by He developed GEFANM. The proposed technology retains the roadway roof by using constant-resistance and large-deformation support technology to cut part of the gob-side roof by using directional cutting technology and forms the roadway side with the caved gangue. In GEFANM, the final settlement amount, rotation angle, and movement intensity of the basic roof are much smaller than those in conventional gob-side entry retention, and several field experiments have been successfully carried out [21–25]. The team led by He successfully carried out field experiments with this new GEFANM technology in the Ningtiaota Coal Mine. This proposed technology is based on GEFANM, but the technology refits the equipment in the working faces and cuts the roadway space with a coal cutter, which can achieve the goal of no pillar retention and fewer driving roadways in all working faces, including the first working face [26–28].

The key block of the basic roof is the main contributor to the structural deformation of the roadway. In the practice of conventional gob-side entry retention, the field monitoring methods for the stability of the basic roof structure have treated the roof and floor convergence of the roadway as a metric [14–19]. The structure of the basic roof in GEFANM is not very different from that of conventional gob-side entry retention. In the study of the basic roof structure, the roof and floor convergence of the roadway was often used as a criterion in the practice of GEFANM [22–24, 26, 27]. Nonetheless, research on the stability of the key block structure of the basic roof with the convergence of the roadway as the only metric is not comprehensive.

This work was set within the engineering context of the GEFANM experiment at the Ningtiaota Coal Mine. The study object was the key block of the basic roof of the roadway. The study described in this paper considered the differences in the caving gob roof on the roof-cutting-line side and examined the structural and mechanical properties of the key block in the field experiment of GEFANM. This study determined the range of the rotation angles when the basic roof structure was stable, and then the bulking coefficient of the gangue on the gravel side based on the rotation angles was calculated. The bulking coefficient on the roadway gravel side was used as the metric in the monitoring method, and the stability of the key block structure of the basic roof was demonstrated according to the bulking coefficient obtained from the observation station. The monitoring results of the bulking coefficient were verified based on the roof and floor convergence data, and the stability of the key block structure of the basic roof was analyzed in a comprehensive way.

2. Project Overview

The GEFANM experiment was carried out in the Ningtiaota Coal Mine, which is located in the middle part of Shenmu County, Yulin City, Shaanxi Province, China. The coal seam considered in the GEFANM experiment is a 2-2 coal seam; this coal seam occurrence is stable, and its dip angle is nearly horizontal. In the working face (S1201-II) of the GEFANM experiment, the dipping length is 280 m, the burial depth is approximately 143.88 m, and the average thickness of the coal seam is 4.04 m. The gob-side entry (airway return way of S1201-II) in the GEFANM experiment is 2,344 m long, and its layout is shown in Figure 1.

GEFANM cuts off the pressure transmission between parts of mine roofs by using directional cutting technology and forms a gob-side entry roof with some of the roof rocks, thereby reducing the stress concentration and periodic pressure on the roof. The roof of the gob on the cutting line side was caved layer by layer; when the gob is not filled with gangue, a sufficient temporary support system can be used to prevent the basic roof from rotating to a large angle. A constant-resistance and large-deformation anchor (CRLDA) cable is used to anchor the roof of the roadway at a height below the cutting line into the basic roof in GEFANM, thereby achieving the goal of safe noncoal mining. According to the stratum characteristics of the S1201-II working face, each section of the gob-side entry is 6 m wide and 3.75 m high, the length and angle of the roof-cutting line are designed as 9 m and 10°, respectively, 5 CRLDA cables are arranged at the top of the roadway, the gangue support is provided at the gravel side, and 3 fiber-reinforced plastic (FRP) bolts are provided at the coal side. The temporary support system is composed of 1 temporary roof-cutting support, 4 hydraulic props, and 2 steel girders. For more details, see Figure 2.

The working process of GEFANM on the S1201-II working face mainly includes the principle of integrated coal side formation, CRLDA cable support, and directional cutting technology. The principle of integrated coal side formation is as follows: as shown in Figure 3(a), when the coal cutter moves to the coal body of the retained roadway and the front drum of the coal cutter is used to slowly set the cutter down until it approaches the coal seam floor, the roadway space is retained. The CRLDA cable support is as follows: as shown in Figure 3(b), under the support of the drilling machine, CRLDA cables are mounted on the roof of the retained roadway to help retain the roadway roof. The directional cutting technology is implemented as follows: to perform directional cutting on the roof on one side of the roadway-retaining gob, as shown in Figure 3(c), to ensure that the roof on one side of the gob cave is along the cutting line face can accommodate the self-weight stress and mining pressure. The temporary support system supports the roadway roof, and the system ensures that the extent of roof settlement does not increase before the roof of the gob fully caves. The coal body, the dense gangue, and the roof supported by the CRLDA cables form a gob-side entry, with the polymer material sealing the gravel side of the roadway to prevent air leakage in the gob. After the roadway structure becomes stable enough for the temporary support system to be removed, the final result of the formed roadway is as shown in Figure 3(d).

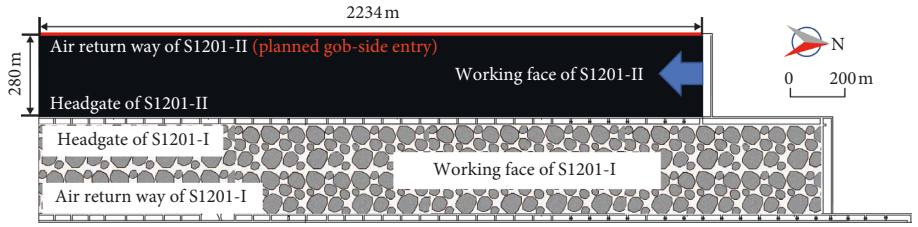

Figure 1: Roadway layout of the S1201-II working face.

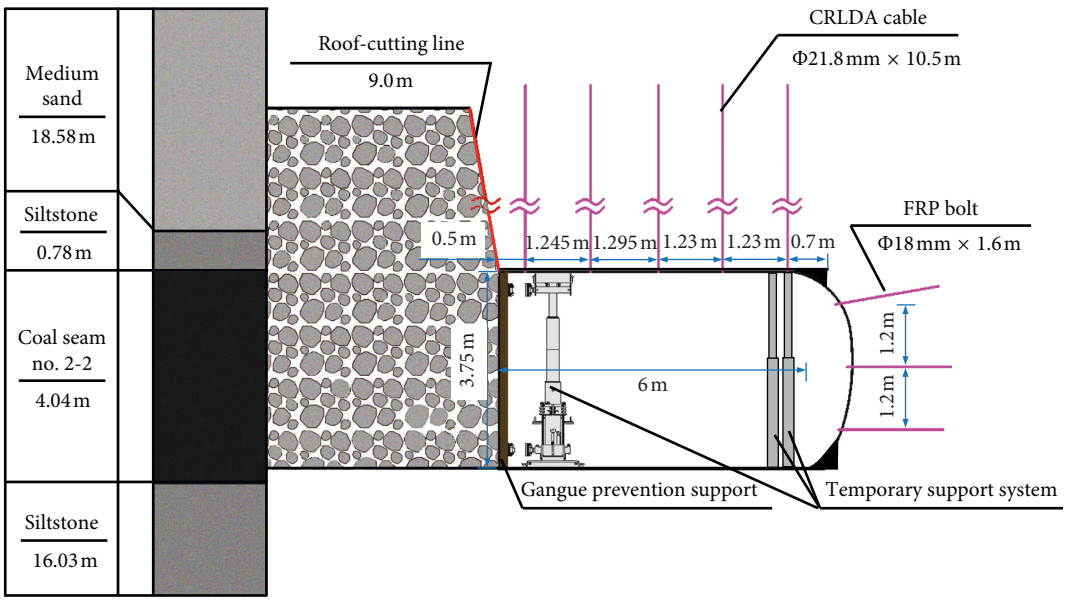

Figure 2: Design of the roof-cutting line and support parameters in GEFANM.

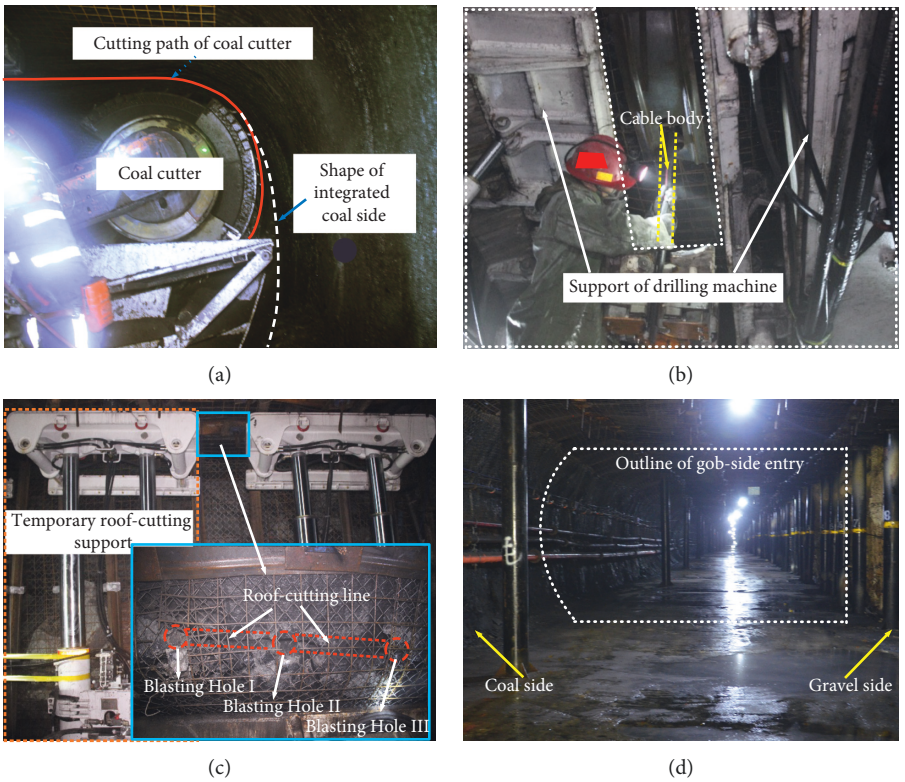

Figure 3: GEFANM process and roadway formation result on the S1201-II working face. (a) Principle of integrated coal side formation. (b) CRLDA cable mounting. (c) Directional roof cutting. (d) Final result of the formed roadway.

3. Stability Analysis of the Key Block of the Basic Roof

3.1. Construction and Analysis of the Mechanical Model. The stability of the basic roof structure depends on the rotation angle of the key block in GEFANM. In the case of complete caving of the roof of the gob at the cutting line side, the roadway roof at a height below the cutting line begins to rotate with the key block. Compared with the case of complete caving of the gob roof at the cutting line side, the key block in the case of partial caving rotates in advance; that is, the key block rotates by a certain angle first. The likelihood of gangue filling the space under the key block varies. Now, assume that if all the gangue fills the space under the key block, then the range of rotation angles at which the key block structure becomes stable can be obtained. If the roof of the gob at the cutting line side does not cave entirely, then the rotation angle of the key block may exceed this range.

Each change in the key block structure is accompanied by the deformation of the space under the key block. For convenience of the mechanical analysis of the key block, the space under the whole key block is divided into bearing areas. As shown in Figure 4, according to the composition of the bearing areas, they can be generally named "Bearing Area I," "Bearing Area II," and "Bearing Area III." Bearing Area I is composed of the coal body and the rock above the coal body; Bearing Area II is composed of the gob-side entry, roadway roof at a height below the cutting line, and temporary support system; Bearing Area III is composed of the gangue in the gob at the cutting line side.

For convenience of calculation, as shown in Figure 5, a coordinate system is established for the key block with O as the coordinate origin, and the key block forms a section (Section B-B view of the key block) along the apex. Once this section becomes unstable, the key block is unstable. The length and thickness of Section B-B are denoted as L_B and h, respectively.

Based on Reference [29], the equation for the length of the key block L_B can be obtained:

$$L_B = l\left(-\frac{l}{S} + \sqrt{\frac{l^2}{S^2} + \frac{3}{2}}\right), \tag{1}$$

where S represents the length of the working face and l represents the periodic roof weighting pace.

The structural diagram of the Section B-B view of the key block and the bearing areas under it is shown in Figure 5, where α is the rotation angle of Section B-B; the contacts at either end of the rock should be equal, the height of the squeezing contact face of the end angle of Section B-B is denoted as s, and given that the roof rocks are in the hinged contact, the action point between the horizontal thrusts is at $s/2$. The action point of Rock A on the OL end of Section B-B is denoted as A, the action point of Rock C on the JN end of Section B-B is denoted as C, the height of the gob-side entry is denoted as h_3, the length of Bearing Area I is denoted as L_1, the length of Bearing Area II is denoted as L_2, the length of Bearing Area III is denoted as L_3, the height of the roof-cutting line is denoted as L_5, and the angle of the roof-cutting line is denoted as θ.

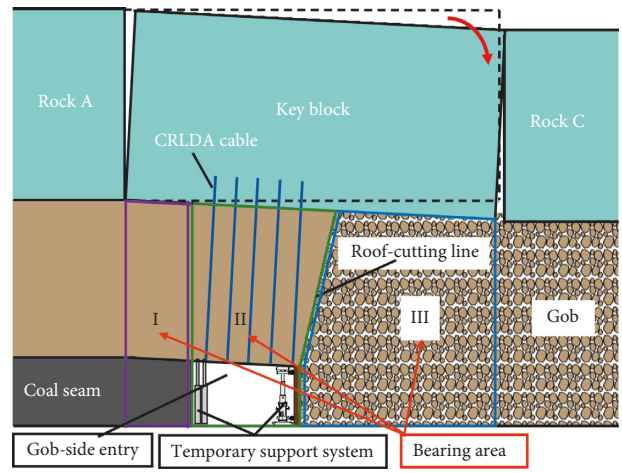

Figure 4: Bearing areas under the key block.

Based on Reference [30], the height of the squeezing contact face of the end angle of the Section B-B view of the key block can be expressed as

$$s = \frac{h - L_B \sin\alpha}{2}. \tag{2}$$

Considering a thicker sand layer in the near-surface area of the studied stratum of the Ningtiaota Coal Mine, the sand layer above the key block is subject to the load-transmitting effect; then, there is a coefficient of load transmission [31]. L_1 is also the width of the stress limit equilibrium area in the coal body. According to Reference [32], an equation for the calculation of L_1 can be obtained:

$$L_1 = \frac{h_3 K_m}{2\tan\varphi_c} \ln\left(\frac{K_G k\gamma_1 H_1 + k\gamma_2 H_3 + c/\tan\varphi_c}{c/\tan\varphi_c + p/K_m}\right), \tag{3}$$

where K_m represents the coefficient of lateral pressure; p represents the coal side support strength; K_G represents the coefficient of load transmission in the sand layer; k represents the coefficient of stress concentration, according to Reference [30], and generally, k is 4; H_1 represents the thickness of the overlying sand layer in the roadway; γ_1 represents the average volumetric force of the overlying sand layer in the roadway; H_3 represents the thickness of the overlying rock layer in the roadway; γ_2 represents the average volumetric force of the overlying rock layer in the roadway; c represents the cohesion between the coal seam and the roof and floor strata; and φ_c represents the internal friction angle between the coal seam and the roof and floor strata.

The length of Bearing Area II is expressed as

$$L_2 = L_g \cos\alpha, \tag{4}$$

where L_g is the initial width of the gob-side entry.

Unlike other bearing zones, Bearing Area III contains loose gangue, and the length L_3 of Bearing Area III changes with the rotation angle α of the key block. Combining equations (1), (3), and (4), we get

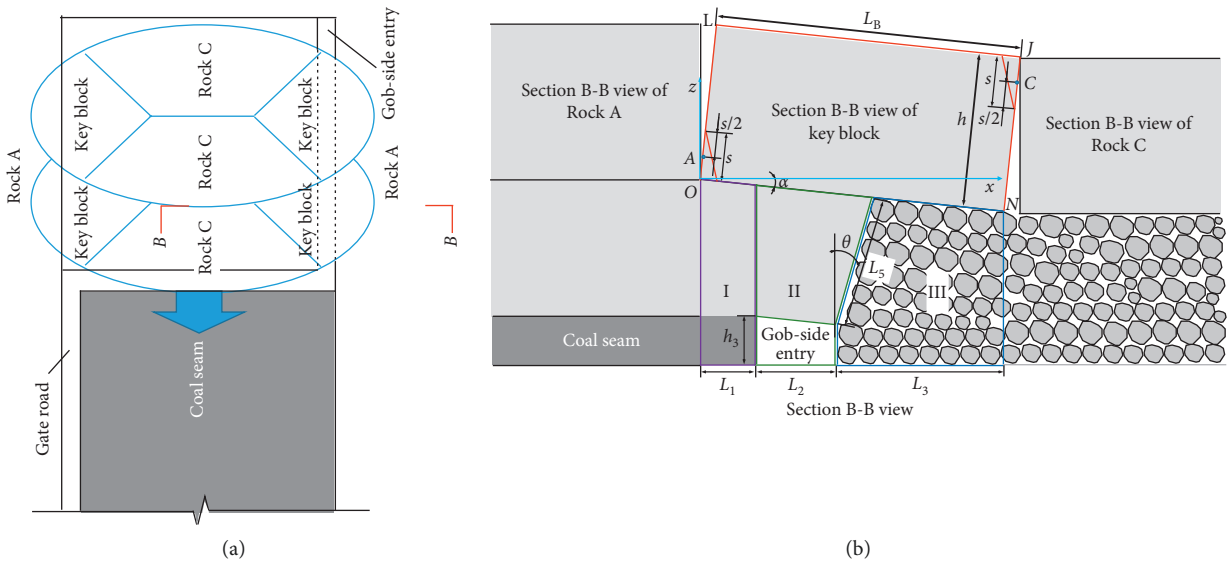

Figure 5: Structural diagram of the key block and bearing zones.

$$L_3 = L_B \cos\alpha - L_1 \cos\alpha - L_2. \quad (5)$$

Based on the field experiment with GEFANM, the stress on the key block is assumed as follows: (1) The key block is a rigid beam, and the rock layer and the sand layer above it evenly cover the key block. (2) The key block rotates around the axis of the border between Bearing Area I and Rock A, rotating and tilting to the gob side, and this border is subject to only the horizontal thrust of Rock A and the vertical support of Bearing Area I. (3) The gangue in Bearing Area III entirely fills the gob. (4) The CRLDA cable support anchors the roadway roof at a height below the cutting line into the key block above it, and the CRLDA cable is subject to only the self-weight stress of the roof at a height below the cutting line instead of the stress applied on the key block.

Based on References [16, 33–36], the stress analysis of the Section B-B view of the basic roof is shown in Figure 6, where the overlying load on Section B-B of Rock A is denoted as q_a, the overlying load on Section B-B of the key block is denoted as q_b, the support load on Section B-B of Rock A is denoted as f_d, the support load of Bearing Area I on Section B-B of the key block is denoted as f_a, the support load of Bearing Area II on Section B-B of the key block is denoted as f, the support load of Bearing Area III on Section B-B of the key block is denoted as f_b, and the support load on Section B-B of Rock C is denoted as f_c. Given that the roof rocks are in the hinged contact, the action point between the horizontal thrusts is at $s/2$, the horizontal force of Rock A applied on Point A at the OL end of Section B-B is denoted as T_a, and the horizontal force of Rock C applied on Point A at the JN end of Section B-B is denoted as T_c. Point C, where Rock C applies the straight force on the squeezing contact face of the end angle of the key block at the JN end of Section B-B, is denoted as Q_{CB}.

The calculation of the load on the overlying stratum should consider the load transmission effect of the overlying

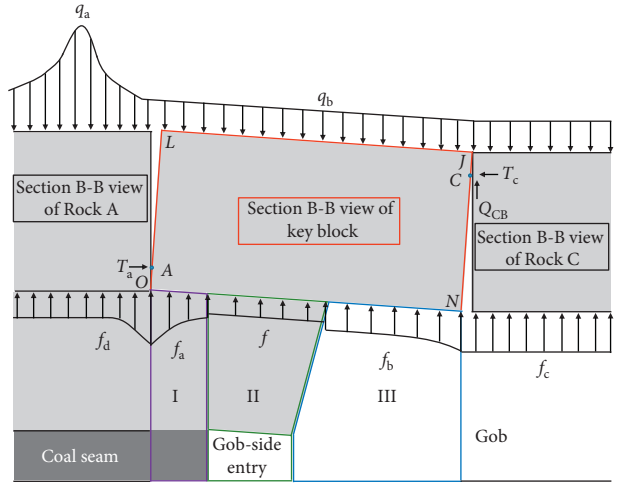

Figure 6: Simplified diagram of the stress on the key block.

sand layer [31]; consequently, q_b is simplified. Then, an equivalent resultant force F_{qb} can be further obtained as

$$F_{qb} = (K_G\gamma_1 H_1 + \gamma_2 H_2) L_B \cos\alpha, \quad (6)$$

where H_2 is the thickness of the overlying rock layer above the key block and γ_2 is the average volumetric force of the overlying sand layer above the key block.

Based on Reference [32], the load f_a that Bearing Area I applies on Section B-B can be idealized as a linearly distributed load [27], and then an equivalent resultant force F_{fa} can be further obtained as

$$F_{fa} = F_{fa1} + F_{fa2} - F_{fa3} = \frac{L_1 \cos\alpha}{2}\left(K_G k\gamma_1 H_1 + k\gamma_2 H_3 - \frac{p}{K_m}\right) + \frac{pL_1 \cos\alpha}{K_m} - \gamma_3 L_5 \cos\theta L_1 \cos\alpha, \quad (7)$$

where γ_3 is the average volumetric force of the roof at the cutting line side.

The temporary support system is composed of 1 temporary roof-cutting support, 4 hydraulic props, and 2 steel girders, and the support load f of Bearing Area II on Section B-B can be considered equivalent to a resultant force F_f.

Considering the stress distribution characteristics of Bearing Area III, the load-bearing force of Bearing Area III on Section B-B is composed of the support load of the gangue in the gob. Based on References [16, 37, 38], considering the differences among the gangues, the average ground coefficient K_{GS} per unit area of gangue is introduced with respect to Section B-B, and the load-bearing force of gangue $F_{f\mathrm{b}}$ can be obtained according to the support load f_{b} generated from the gangue per unit area in Bearing Area III; that is,

$$F_{f_{\mathrm{b}}} = \int_{L_1\cos\alpha + L_2}^{L_1\cos\alpha + L_2 + L_3} K_{\mathrm{GS}} \tan\alpha x \, \mathrm{d}x. \tag{8}$$

The moments of force generated by $F_{q\mathrm{b}}$, $F_{f\mathrm{a}}$, $F_{f\mathrm{b}}$, and F_f against Point A in Section B-B are

$$\begin{aligned}
M_{\mathrm{AF}q\mathrm{b}} &= F_{q\mathrm{b}}\left[\frac{L_{\mathrm{B}}\cos\alpha}{2} + h\sin\alpha - \frac{s\sin\alpha}{2}\right],\\
M_{\mathrm{AF}f\mathrm{a}} &= F_{q\mathrm{a}1}\left(\frac{L_1\cos\alpha}{3} - \frac{s\sin\alpha}{2}\right) + \left[F_{f\mathrm{a}2} - F_{f\mathrm{a}3}\right]\left(\frac{L_1\cos\alpha}{2} - \frac{s\sin\alpha}{2}\right),\\
M_{\mathrm{AF}f} &= F_f\left(L_1\cos\alpha + \frac{L_2}{2} - \frac{s\sin\alpha}{2}\right),\\
M_{\mathrm{AF}f\mathrm{b}} &= \int_{L_1\cos\alpha + L_2}^{L_1\cos\alpha + L_2 + L_3} K_{\mathrm{GS}}\tan\alpha x\left(x - \frac{s\sin\alpha}{2}\right)\mathrm{d}x.
\end{aligned} \tag{9}$$

Let $\sum \underline{F}_z = 0$, $\sum F_x = 0$, and $\sum M_{\mathrm{A}} = 0$; therefore,

$$\begin{aligned}
&F_{q_{\mathrm{b}}} - Q_{\mathrm{CB}} = F_{f_{\mathrm{a}}} + F_{f_{\mathrm{d}}} + F_f,\\
&M_{\mathrm{AF}q\mathrm{b}} - T_{\mathrm{c}}\left(h\cos\alpha - s\cos\alpha - L_{\mathrm{B}}\sin\alpha\right) = M_{\mathrm{AF}f\mathrm{a}}\\
&\quad + M_{\mathrm{AF}f} + M_{\mathrm{AF}f\mathrm{b}} + Q_{\mathrm{CB}}\left(L_{\mathrm{B}}\cos\alpha + h\sin\alpha - s\sin\alpha\right),\\
&T_{\mathrm{c}} = T_{\mathrm{a}}.
\end{aligned} \tag{10}$$

Through calculation, the results can be obtained as

$$Q_{\mathrm{CB}} = F_{q_{\mathrm{b}}} - F_{f_{\mathrm{a}}} - F_{f_{\mathrm{d}}} - F_f, \tag{11}$$

$$\begin{aligned}
T_{\mathrm{c}} = T_{\mathrm{a}} &= \frac{M_{\mathrm{AF}q\mathrm{b}} - M_{\mathrm{AF}f\mathrm{a}} - M_{\mathrm{AF}f} - M_{\mathrm{AF}f\mathrm{b}}}{h\cos\alpha - s\cos\alpha - L_{\mathrm{B}}\sin\alpha}\\
&\quad - \frac{\left(F_{q_{\mathrm{b}}} - F_{f_{\mathrm{a}}} - F_{f_{\mathrm{d}}} - F_f\right)\left(L_{\mathrm{B}}\cos\alpha + h\sin\alpha - s\sin\alpha\right)}{h\cos\alpha - s\cos\alpha - L_{\mathrm{B}}\sin\alpha}.
\end{aligned} \tag{12}$$

3.2. Analysis of Stability. The instability of the key block structure can be inferred from the structure of Section B-B (view of the key block). Once Section B-B becomes unstable, the key block becomes unstable. As shown in Figure 5, the *OL* end of Section B-B is mounted on Bearing Area I and rotates around it as the axis, and the structure at the end is relatively stable. In contrast, the *JN* end of Section B-B is supported by Bearing Area III, the gangue in Bearing Area III is compressed continuously, and the structure at this end is unstable. As the gangue is compressed, the *JN* end of Section B-B does not slide along the contact face; that is, Section B-B does not rotate. In this case, the key block structure is stable. If the rotation angle of Section B-B continues to increase, the contact face area at the *JN* end of Section B-B decreases. When the force applied on the contact face is more than the ultimate strength, the contact face is crushed. Section B-B does not come into contact with Rock C and is subject to rotation instability.

Based on Reference [30], the criterion for Section B-B to stop sliding is

$$T_{\mathrm{c}} \tan\varphi_{\mathrm{r}} \geq Q_{\mathrm{CB}}, \tag{13}$$

where $\tan\varphi_{\mathrm{r}}$ represents the coefficient of friction between the contact faces at the *JN* end of Section B-B.

Combining equations (11)–(13), the sliding force F_S on Section B-B is defined; that is,

$$F_S = T_{\mathrm{c}} \tan\varphi_{\mathrm{r}} - Q_{\mathrm{CB}}. \tag{14}$$

The following can be further obtained: the sliding force F_S on Section B-B increases with increasing rotation angle α. If $F_S \geq 0$, Section B-B stops sliding; if $F_S < 0$, Section B-B continues to slide.

Combining Reference [30], the criterion for preventing rotation instability in Section B-B is

$$T_{\mathrm{c}} \leq s\eta\sigma_{\mathrm{c}}, \tag{15}$$

where $\eta\sigma_{\mathrm{c}}$ represents the ultimate strength between the contact faces at the *JN* end of Section B-B.

Combining equations (12) and (15), the rotation force F_R on Section B-B is defined as

$$F_R = T_{\mathrm{c}} - s\eta\sigma_{\mathrm{c}}. \tag{16}$$

Additionally, the rotation force F_R on Section B-B increases with increasing rotation angle α. If $F_R > 0$, then rotation instability occurs; if $F_R \leq 0$, then rotation instability does not occur.

The above mechanical analysis is performed with the assumption that the roof of the gob at the cutting line side is entirely caved. When the roof of the gob at the cutting line side is partially caved, Section B-B rotates by a certain angle before contacting gangue. Compared with the entire roof of the gob caving at the cutting line side, the results show that the rotation angle increases, F_S increases, the sliding time of Section B-B increases, the contact face area at the *JN* end of Section B-B decreases, and F_R increases, which means that Section B-B is more vulnerable to rotation instability.

An integrated analysis suggests that when the roof of the gob at the cutting line side is entirely caved, if the sliding force of Section B-B $F_S \geq 0$ and the rotation force $F_R \leq 0$, the rotation angle should change within a certain range, which should reflect the safe range of the rotation angle of the key block. When the roof of the gob at the cutting line side is partially caved, if the rotation angle of the key block falls

within this range, then the key block structure tends to be more stable; if the angle is outside this range, then the key block structure is more vulnerable to instability.

4. Monitoring Method

The stability of the key block of the basic roof is mainly linked to the rotation angle, but the field engineering environment is very complex; it is relatively difficult to obtain the variation in the rotation angles of Section B-B. In the study of the basic roof structure, roof and floor convergence of the roadway was often used as a criterion in the practice of GEFANM [22–24, 26, 27]. However, the analysis of the stability of the key block structure simply based on the deformation of the gob-side entry is relatively lenient. The author seeks an innovative monitoring metric to infer the rotation angle of the key block and evaluate the stability of the key block structure.

Combining the movement characteristics of the key block, the increase in the rotation angle (α) of Section B-B mainly depends on the settlement (Δh) at the *JN* end:

$$\alpha = \arcsin\left(\frac{\Delta h}{L_{\mathrm{B}}}\right). \tag{17}$$

With the rotation of Section B-B around the *OL* end, the settlement increases, the compression of the gob-side gangue near the roadway increases, and the compression change in the gob-side gangue is mainly linked with the change in its bulking coefficient. In addition, the gob-side gangue is in a loose state, which can uniformly transfer the overlying stress to every piece of gangue; thus, it is easier to observe the bulking phenomenon of gangue at the gravel side of the roadway. Assume that the gob-side gangue is uniformly compressed. Given the differences in the lithological character, the authors attempt to infer how the rotation angle (α) of Section B-B changes by monitoring the variation in the average bulking coefficient of the gangue at the gravel side. Assume that the roof of the gob on the cutting line side is entirely caved; then, the average bulking coefficient K_{GB} on one side of the gravel of the roadway is

$$K_{\mathrm{GB}} = \frac{h_3 + L_5\cos\theta - \Delta h_f - \left(L_1 + L_{\mathrm{g}} + L_x\right)\sin\alpha}{L_5\cos\theta}, \tag{18}$$

where L_x is the average width of the gangue at the gravel side and Δh_f is the floor heave at the gangue side of the roadway.

In summary, a monitoring method for the average bulking coefficient at the gravel side of the roadway is proposed. When the gob roof at the cutting line side is entirely caved, the proposed method can be used to obtain the safe range of the rotation angle of the key block; then, the range of safe average bulking coefficients of gangue may be inferred from the safe range of the rotation angle. Assume that the gob roof at the cutting line side is partially caved; if the average bulking coefficient of the gangue falls within this range, then the key block structure tends to be more stable; if the bulking coefficient is outside this range, then the key block structure is more vulnerable to instability.

5. Field Monitoring Case Study

5.1. Calculation of Parameters. The parameters used to represent the S1201-II working face of the Ningtiaota Coal Mine are as follows: combined with engineering geological data and GEFANM experimental design parameters, it can be concluded that $S = 280$ m, $l = 18$ m, $h_3 = 3.75$ m, $L_{\mathrm{g}} = 6$ m, $\gamma_1 = 18 \times 10^3$ N/m^3, $F_f = 4800$ kN, $\gamma_2 = 27 \times 10^3$ N/m^3, $H_1 = 45.54$ m, $H_2 = 78.98$ m, $H_3 = 98.34$ m, $\gamma_3 = 27 \times 10^3$ N/m^3, $c = 0.85$ MPa, $\varphi_{\mathrm{c}} = 36.69^\circ$, $L_5 = 9$ m, $\theta = 10^\circ$, $p = 0.048$ MN, and $\sigma_{\mathrm{c}} = 22.7$ MPa; the engineering background of some references is similar to the GEFANM experimental background, and combined with the experimental data of References [30–32, 37], it can be concluded that $K_{\mathrm{m}} = 0.65$, $\eta = 0.4$, $K_{\mathrm{GS}} = 10$ MN/m, $\varphi_{\mathrm{r}} = 26.6^\circ$, and $K_{\mathrm{G}} = 0.93$. Thus, the sliding force and the rotation force of Section B-B are calculated for when the gob roof at the cutting line side is entirely caved. Assume that the bulking coefficient of the gangue under the *JN* end of Section B-B is compressed to 1.0 and that the rotation angle limit of the key block is 11°.

To explore the relationship between the rotation angle of Section B-B and the structural instability of the key block, when the roof of the gob at the cutting line side is entirely caved, the sliding force and the rotation force increase with increasing rotation angle of Section B-B. As shown in Figure 7, the safe range of the rotation angle of Section B-B is 0.9–2.1°. When the roof of the gob at the cutting line side is partially caved, if the rotation angle of Section B-B still falls within the safe range, then the structure of the key block is also stable; if the rotation angle of Section B-B is outside this range, then the key block structure is relatively vulnerable to instability.

The parameters used to represent the S1201-II working face of the Ningtiaota Coal Mine are as follows: $\Delta h_f = 0$ m and $L_x = 1$ m. A variation trend graph is plotted for the rotation angle of Section B-B and for the average bulking coefficient of the gangue at the gravel side of the roadway.

Considering the abovementioned analysis, the relationship between the rotation angle of Section B-B and the average bulking coefficient of the gangue at the gravel side of the roadway is shown in Figure 8. As the rotation angle increases, the average bulking coefficient of the gangue decreases. Combining the safe range of the rotation angle of the key block, the range of safe average bulking coefficients of gangue at the gravel side of the roadway is identified as 1.40–1.37. When the roof of the gob at the cutting line side is partially caved, the average bulking coefficient of the gangue at the gravel side is still within the range 1.40–1.37, and the key block structure is also stable. When the average bulking coefficient of the gangue is less than 1.37, the key block structure is more vulnerable to instability.

5.2. Field Research Scheme. The field research scheme is intended to reveal how the rotation angle of Section B-B changes by observing the variation in the bulking coefficient of the gangue at the gravel side of the roadway, which can indicate the stability of the key block structure. In the experiment with the S1201-II working face of the Ningtiaota

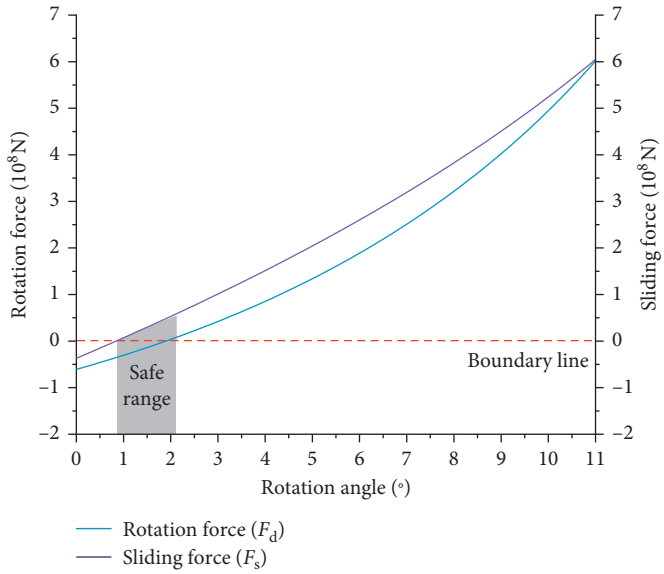

Figure 7: Relationship between sliding force, rotation force, and rotation angle of Section B-B (view of the key block).

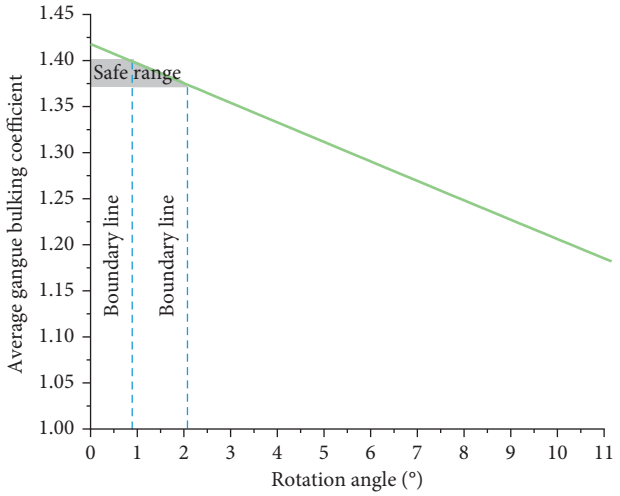

Figure 8: Relationship between the average gangue bulking coefficient and the rotation angle.

Coal Mine, the gob roof on the cutting line side was caved layer by layer; the first layer was generally caved from the higher level, and the heap of the gangue is very high—up to three-fourths the height of the roadway. The initial bulking coefficient may vary spatially but ultimately conforms to the monitoring principle. Considering the field engineering background, a set of field monitoring schemes for the stability of the key block structure based on the bulking effect at the gravel side of the roadway was implemented. As mentioned, the work aimed to determine the same roof-cutting line parameters, to analyze how the average bulking coefficient of the gangue changes, and to investigate the stability of the key block structure in GEFANM.

As mentioned above, when the roof of the gob at the roof-cutting-line side was partially caved, the sufficient temporary support system ensured that the basic roof would not rotate by a large angle; however, the temporary support at 778–900 m from the beginning of the roadway was reduced. In the process of GEFANM, the roof of the gob at the cutting line side was caved layer by layer. For convenience of research on the bulking coefficient of the gangue below Section B-B of the key block in the field, the area in the first layer with a height of caved gangue less than the height of the roadway was selected as the monitoring station, the gravel side in the area of the observation stations was not sealed with polymer materials, and 7 observation stations were provided for the scheme. The configuration is shown in Figure 9(a), including Station I (342 m from the beginning of the roadway), Station II (468 m from the beginning of the roadway), Station III (522 m from the beginning of the roadway), Station IV (648 m from the beginning of the roadway), Station V (738 m from the beginning of the roadway), Station VI (828 m from the beginning of the roadway), and Station VII (864 m from the beginning of the roadway). Temporary support system I for the roadway located at Station I, Station II, Station III, Station IV, and Station V was composed of 1 temporary roof-cutting support, 4 hydraulic props, and 2 steel girders; the spacing between the girders was 1.2 m. Temporary support system II for the roadway located at Station VI and Station VII was less intense and included 1 temporary roof-cutting support, 2 hydraulic props, and 1 steel girder; in this case, the spacing between the girders was 2.4 m. The observation instruments included a laser range finder (LRF), LRF tripod, observation platform, slope gauge, and tape measure.

The field observations from the monitoring scheme are shown in Figure 9(b). The layout of the observation instruments is shown in Figure 10(a). In the roadway at a height of h_3, the LRF (at a height of h_{LR}) was laid out by the observation platform; to obtain the original thickness of the roof caving area, the length of the key block hanging at the gob side L_3 was calculated from the field parameters. Within the range of L_3, subject to the limitation of the erected platform, the first point that could be obtained by the LRF

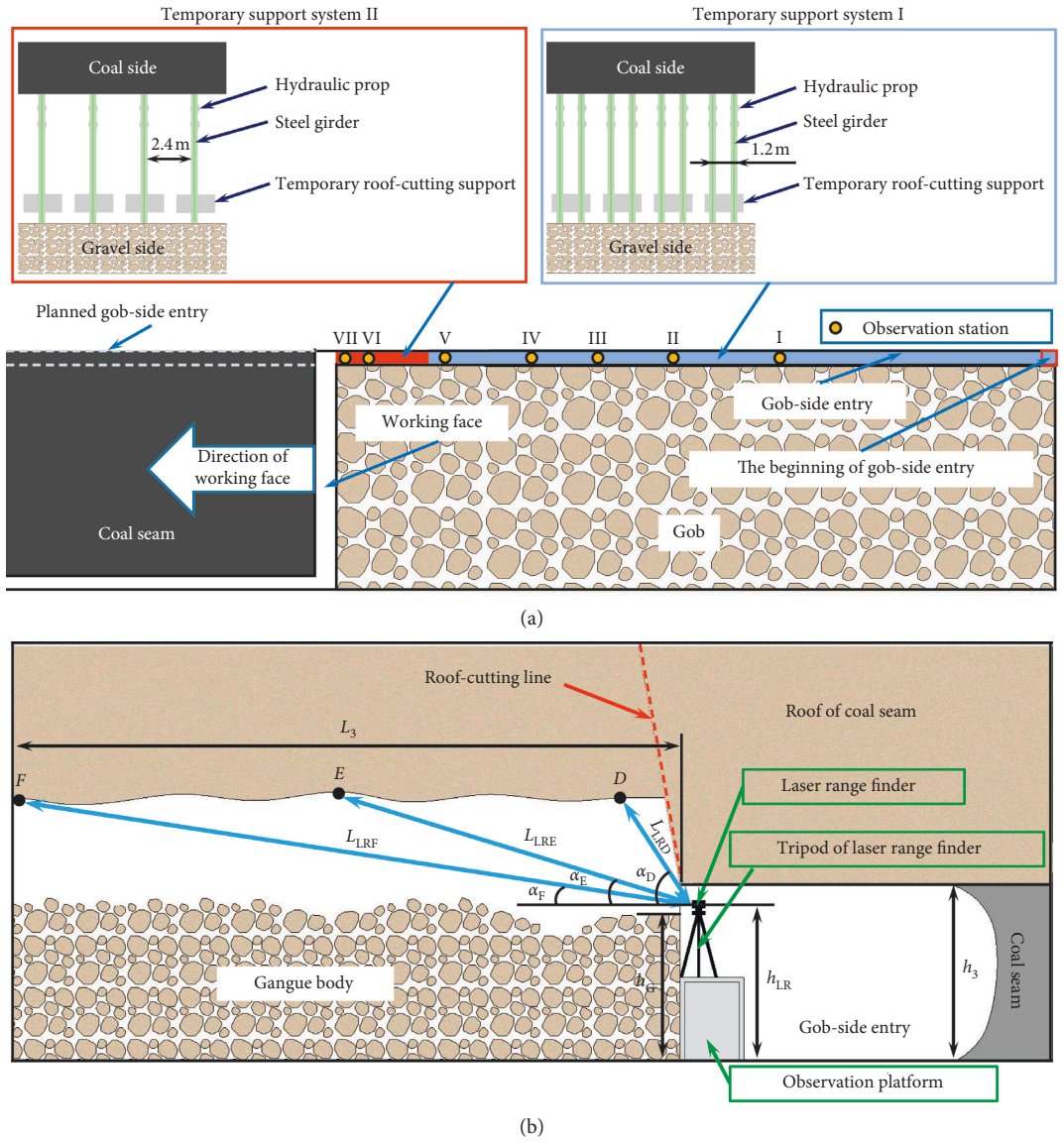

FIGURE 9: Diagram of the field monitoring scheme. (a) Diagram of the layout of the observation stations. (b) Diagram of the field observations in the monitoring scheme.

from the area without caving roof was marked as D. The center of L_3 was marked as E. The end position of L_3 was marked as F. The line distances from $D/E/F$ to the LRF were $L_{LRD}/L_{LRE}/L_{LRF}$, respectively, and were acquired with the LRF. The horizontal angles of $L_{LRD}/L_{LRE}/L_{LRF}$ were $\alpha_D/\alpha_E/\alpha_F$, respectively, and were measured with a slope gauge. The average original thickness of the caved roof area can be obtained from the data in relation to these three points; as shown in Figures 10(b) and 10(c), an observation line was provided in the highest gangue at the gravel side, the height of the gangue at the gravel side h_G was observed daily, and the data were calibrated with the LRF and tape measurements.

This scheme summarized the daily data obtained from every observation station; then, the daily average bulking coefficient of the gangue at the gravel side K_{GB} was calculated:

$$K_{GB} = \frac{3h_G}{L_{LRD}\sin\alpha_D + L_{LRE}\sin\alpha_E + L_{LRF}\sin\alpha_F + 3h_{LR} - 3h_3}. \quad (19)$$

5.3. Analysis of the Results. This study selected the data of the average bulking coefficient of the gangue on the gravel side of the roadway obtained from each observation station daily, combined with the distance of the hysteretic working surface from the observation stations, to plot the relational graph of the average gangue bulking coefficient and the distance of the hysteretic working surface. Analysis of the variation trend of the average gangue bulking coefficient at the gravel side of the roadway with the distance of the hysteretic working surface, combined with the results obtained from theoretical calculations, was used to

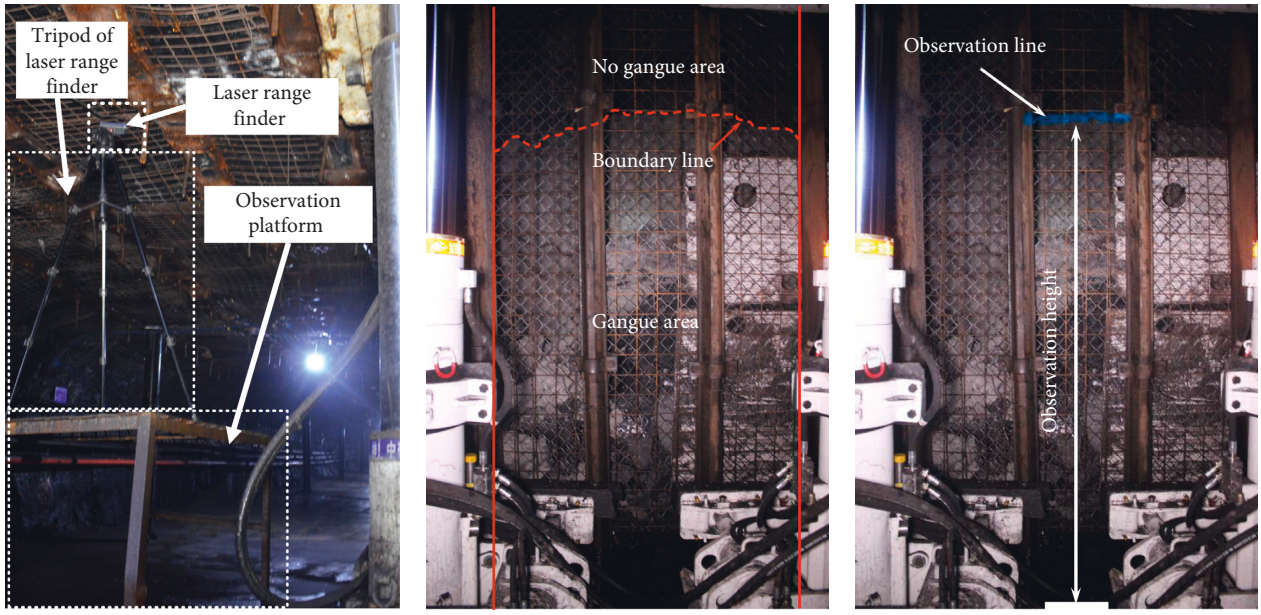

Figure 10: Field observation diagram relative to the study plan of the bulking coefficient. (a) Layout of the observation instruments. (b) Caving of gangue at the observation stations. (c) Observation line and height diagram.

examine the stability of the key block structure above the observation stations.

The relationship between the average bulking coefficient of the gangue at the gravel side and the distance of the hysteretic working face is shown in Figure 11. The results of the analysis of the variation trend of the bulking coefficient include the following: (1) As the distance from the hysteretic working face increased, the average bulking coefficient of the gangue decreased, and the variation in the bulking coefficient obtained from all observation stations tended to be stable within 200 m of the hysteretic working face. (2) When the distance from the hysteretic working face was 150 m, the stability range of the data of the bulking coefficient obtained from Station I, Station II, Station III, Station IV, and Station V was 1.38–1.37, the stability values fell within the safe range calculated from the parameters, and the key block structure within the area of these observation stations was stable. (3) When the distance of the hysteretic working face was 110 m, the bulking coefficients obtained from Station VI and Station VII were 1.37, which was much smaller than that obtained from any other station and tended to further decrease, easily beyond the range of safe average bulking coefficients calculated from the parameters; to prevent the key block structure from becoming unstable, supplementary support scheme I was implemented on the roadway; that is, the hydraulic prop was replaced by a temporary roof-cutting support in every other row. (4) When the distance of the hysteretic working face was 130 m, the bulking coefficients obtained from Station VI and Station VII were smaller than those from any other station, and the bulking coefficient obtained from Station VII was 1.36, which deviated from the range of safe average bulking coefficients obtained from the theoretical calculation; thus, the key block structure was relatively vulnerable to instability. In this case, supplementary support scheme II was implemented on the roadway; that is, 1 steel girder and 4 hydraulic props were supplemented between every set of temporary roof-cutting supports, and some supplementary flexible-formwork concrete pillars were added. (5) In supplementary support scheme II, after reaching a distance of 170 m from the working face, the bulking coefficients obtained from Station VI and Station VII finally tended to stabilize, but the final bulking coefficients were 1.35 and 1.34, respectively; thus, the key block structure was still highly vulnerable to instability.

6. Discussion

The traditional mining technology wastes coal pillar resources and requires two roadways to be constructed in advance. The conventional gob-side entry technology could solve the problems existing in traditional mining technology, but the roadway pressure is high and support cost must be increased. GEFANM technology could solve the problems existing in the conventional gob-side entry technology. The key block of the basic roof is the main contributor to the structural deformation of the roadway, and the structural characteristics of the key block are critical to the stability of the gob-side entry in GEFANM. The stability research for the key block structure of the basic roof of GEFANM has great significance for application and promotion of this technology. In the research on the stability of the basic roof structure, the roof and floor convergence of the roadway was often used as a criterion in the practice of GEFANM [22–24, 26, 27]. In this study, combined with the theoretical calculation results, it can be concluded that the key block

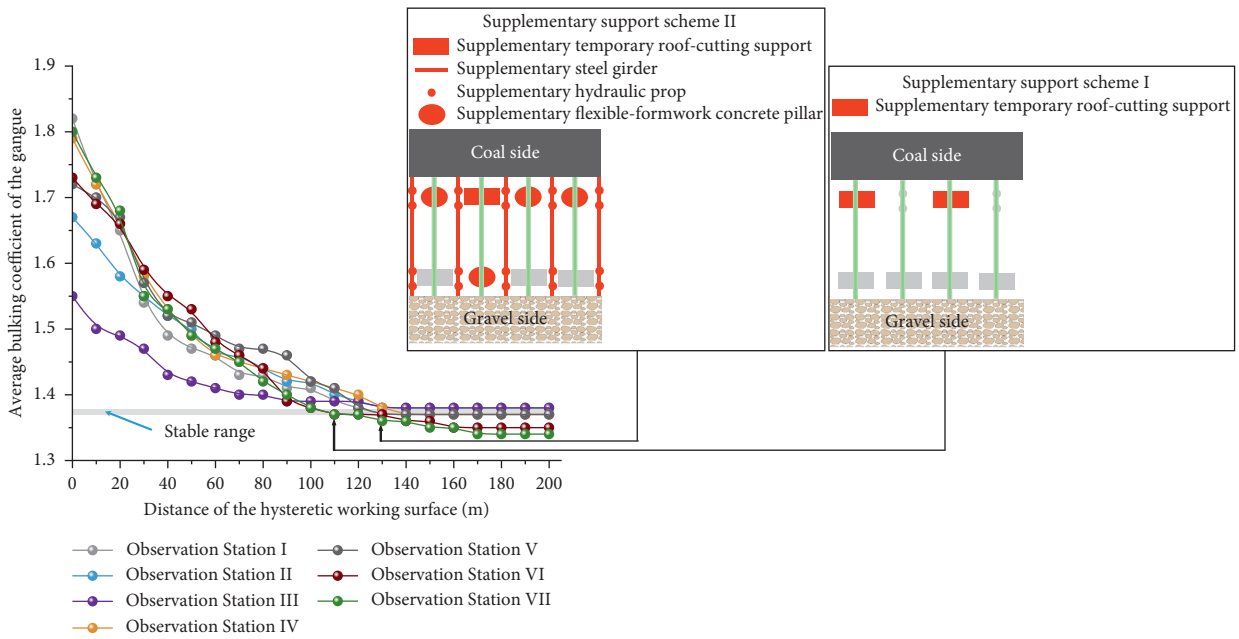

Figure 11: Relationship between the bulking coefficient of the gangue and the distance of the hysteretic working face.

structure is in a stable state when the rotation angle of the key block is within a range. With the rotation of the key block structure, the compression of the gob-side gangue also increases. This study carried out field monitoring for the bulking effect at the gravel side of the roadway, and the stability of the key block structure of the basic roof was inverted by the change of the bulking coefficient of the gangue.

The stability analysis of the key block suggests that the structural stability of the key block mainly depends on the status of the gangue in the gob. The gangue has the effect of bulking; as the key block structure rotated, the bulking coefficient of the gangue decreased. As the gangue is compressed, the end of the key block does not slide along the contact face and the key block does not rotate. In that time, the bulking coefficient of the gangue cannot change. If the rotation angle of the key block continues to increase, then the contact face area at the end of the key block decreases. When the force applied on the contact face is more than the ultimate strength, the contact face is crushed and the key block is subject to rotation instability. The bulking coefficient of the gangue can also be used as a monitoring metric to estimate the stability of the key block structure, and the safe range of the bulking coefficient of the gangue is deduced via theoretical calculation. The field monitoring results showed that the key block structure was stable when the bulking coefficient of the gangue fell within the safe range. To verify the scientific nature of the field monitoring scheme, the monitoring data of the roof and floor convergence at the center of the roadway obtained from each observation station were introduced as supporting evidence, and the relationship between the roof and floor convergence in the center of the roadway and the distance of the hysteretic working face was plotted to validate the scientific nature of the field monitoring scheme.

The relationship between roof and floor convergence in the center of the roadway and the distance of the hysteretic working face is shown in Figure 12. Based on an analysis of how roof and floor convergence in the center of the roadway changes within 200 m of the hysteretic working face, the following results were obtained: (1) Roof and floor convergence in the center of the roadway increased with increasing distance of the hysteretic working face; roof and floor convergence in Station I, Station II, Station III, Station IV, and Station V basically stabilized after reaching a distance of 150 m from the working face, and the range of stable values of the roof and floor convergence was mainly from 95 mm to 113 mm. In this stage, the key block structure in the roof of the roadway was stable, without cracks. (2) When the distance of the hysteretic working face was 110 m, the roof and floor convergence in Station VI and Station VII was large, but the maximum deviation from that of any other station was 22 mm. Supplementary support scheme I was implemented on the roadway, but the deviation from the data obtained from these two stations to those obtained from other stations still tended to increase. (3) When the distance of the hysteretic working face was 130 m, supplementary support scheme II was implemented on the roadway, but its maximum deviation from that of any other station was 34 mm. (4) Farther than 170 m from the working face, under the conditions of supplementary support scheme II, the convergence at Station VI and Station VII tended to be stable, but the maximum deviation of the final deformation from that of any other station was 66 mm. Cracks were observed on the roof at Station VI and Station VII, and the key block structure was relatively vulnerable to instability.

Through comparison and discussion of the results of the stability analysis of the key block, the bulking coefficient of the gangue, and the roof and floor convergence in the center of the roadway, the results show that when the stable gangue

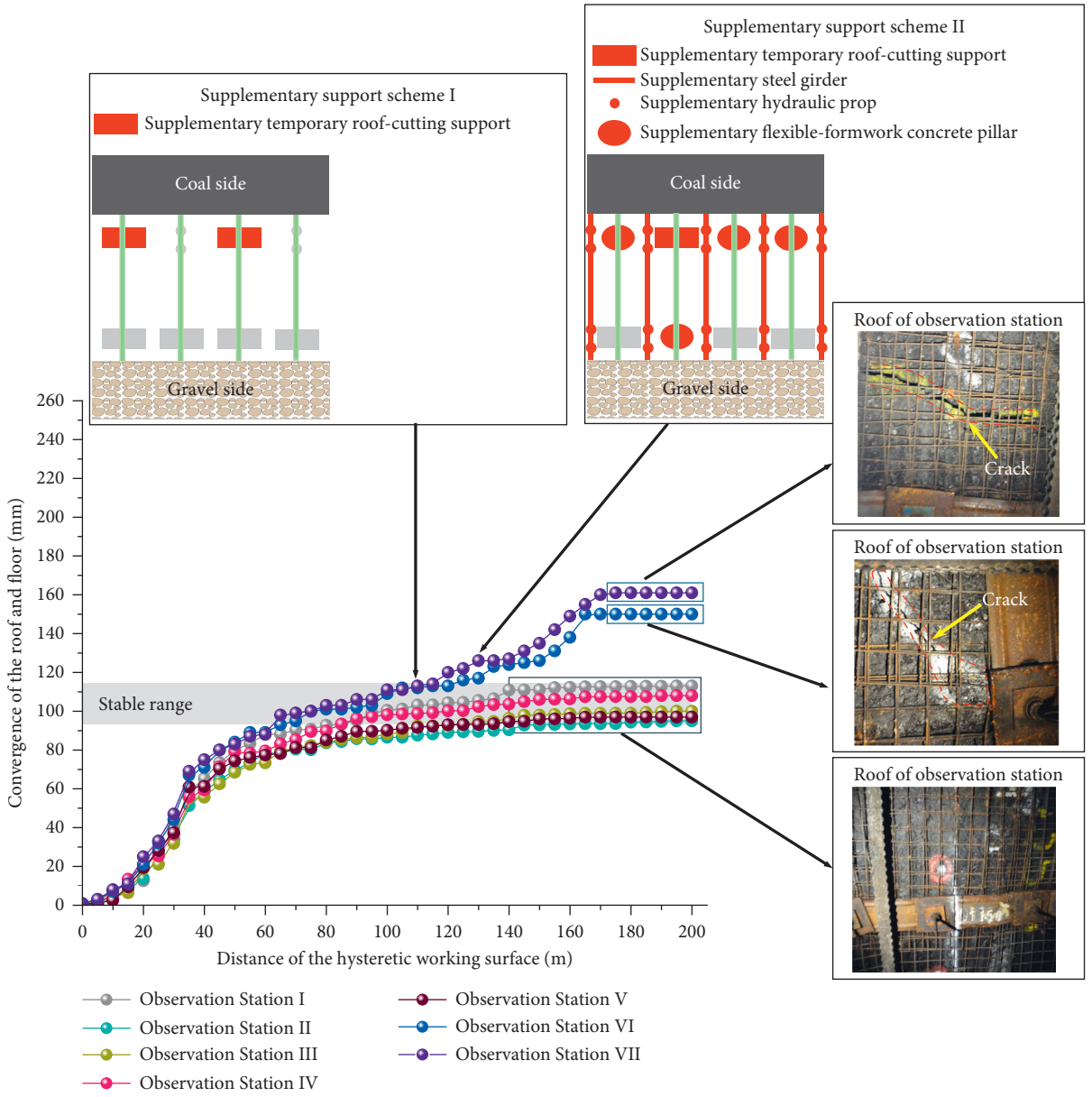

Figure 12: Relationship between roof and floor convergence in the center of the roadway and the distance of the hysteretic working face.

bulking coefficient fell within the safe range calculated from the parameters, the key block structure of the basic roof was relatively stable. When the bulking coefficient was outside this range, the roof and floor convergence in the center of the roadway was large, and cracks were observed on the roof, which verified that the bulking coefficient of the gangue can be used as an innovative monitoring metric to study the stability of the key block structure.

In other words, the bulking coefficient of the gangue in the gob directly reflects the stability of the key block structure. In future research, the bulking coefficient of the gangue can be taken as one of the evaluation criteria for the stability of the key block in the GEFANM experiment. However, the engineering geological condition that this paper relies on is relatively simple and buried at a shallow depth, the stratum of this GEFANM experiment is stable, and its dip angle is nearly horizontal. The structure and mechanical state of gangue in the gob are relatively loose and easy to change under the influence of the engineering geological condition. However, the monitoring method for the gangue bulking coefficient and stability analysis of the key block structure of the basic roof of GEFANM is successfully implemented in the coal seam with a shallow buried depth and simple engineering geological condition. According to the complicated engineering geological condition of the coal seam, the study on the bulking coefficient of the gangue should be further improved step by step. In the future, research on methods for gangue bulking coefficient monitoring and stability analysis should focus on the GEFANM experiment with complicated engineering geological conditions.

7. Conclusion

In this study, by analyzing the stability of the key block of the basic roof, the safe range of the rotation angle was identified. By establishing the monitoring method for the bulking coefficient of the gangue at the gravel side as the metric, regardless of whether the roof of the gob at the cutting line side is entirely caved, the range of the safe average bulking coefficients of gangue may be inferred from the safe range of the rotation angle. If the average bulking coefficient of the gangue falls within this range, then the key block structure tends to be stable; if it falls outside this range, then the key block structure is relatively vulnerable to instability.

By introducing the field parameters, the safe range of rotation angles of the key block was determined to be 0.9–2.1°, and the range of safe average bulking coefficients of gangue was determined to be 1.40–1.37. After implementation of the field monitoring scheme, the monitoring results showed that the range of stable values of the bulking coefficient was 1.38–1.37, which fell into the safe range calculated from the parameters. In this area, the main range of the stable values of the roof and floor convergence of the roadway was 95–113 mm, and there was no crack observed on the roof of the roadway, indicating that the key block structure in this area was stable. When the temporary support was reduced, the corresponding bulking coefficient was less than that with the original support during the same period. Even with two supplementary support schemes, the final bulking coefficients were 1.35 and 1.34, and the bulking coefficient tended to be stable; however, it exceeded the safe range obtained from the parameter calculation. The maximum deviation between this area and any other observation station was 66 mm, and cracks were observed on the roof. There was a relatively large likelihood of instability of the key block structure.

The monitoring results of the gangue bulking coefficient and the field monitoring data of the roof and floor convergence validate the theoretical calculation results. The gangue bulking coefficient can be used as an innovative monitoring metric to study the stability of the key block structure of the basic roof.

Data Availability

The data used to support the findings of this study are available from the corresponding author upon request.

Conflicts of Interest

The authors declare that they have no conflicts of interest.

Acknowledgments

This work was supported by the National Key R&D Program (no. 2016YFC0600900) and the National Natural Science Foundation of China (nos. 51904207 and 51674265), which are gratefully acknowledged.

References

[1] M. Himley, "Global mining and the uneasy neoliberalization of sustainable development," *Sustainability*, vol. 2, no. 10, pp. 3270–3290, 2010.

[2] D. Laurence, "Establishing a sustainable mining operation: an overview," *Journal of Cleaner Production*, vol. 19, no. 2-3, pp. 278–284, 2011.

[3] W. Wang and C. Zhang, "Evaluation of relative technological innovation capability: model and case study for China's coal mine," *Resources Policy*, vol. 58, pp. 144–149, 2018.

[4] P. F. Shan, X. P. Lai, and X. M. Liu, "Correlational analytical characterisation of energy dissipation-liberation and acoustic emission during coal-rock mass fracture inducing by coal excavation," *Energies*, vol. 12, no. 12, p. 2382, 2019.

[5] P. F. Shan and X. P. Lai, "Numerical simulation of the fluid-solid coupling process during the failure of a fractured coal-rock mass based on the regional geostress," *Transport in Porous Media*, vol. 124, no. 3, pp. 1061–1079, 2018.

[6] H. Sun, X. L. Liu, and J. B. Zhu, "Correlational fractal characterisation of stress and acoustic emission during coal and rock failure under multilevel dynamic loading," *International Journal of Rock Mechanics and Mining Sciences*, vol. 117, pp. 1–10, 2019.

[7] P. Wang, L.-s. Jiang, P.-q. Zheng, G.-p. Qin, and C. Zhang, "Inducing mode analysis of rock burst in fault-affected zone with a hard-thick stratum occurrence," *Environmental Earth Sciences*, vol. 78, no. 15, p. 467, 2019.

[8] Y. Zhang, Z. Wan, F. Li et al., "Stability of coal pillar in gob-side entry driving under unstable overlying strata and its coupling support control technique," *International Journal of Mining Science and Technology*, vol. 23, no. 2, pp. 193–199, 2013.

[9] H. Li, P. Syd, H. Li et al., "Trial of small gateroad pillar in top coal caving longwall mining of large mining height," *International Journal of Mining Science and Technology*, vol. 26, no. 1, pp. 139–147, 2016.

[10] F. Wang and C. Zhang, "Reasonable coal pillar design and remote control mining technology for highwall residual coal resources," *Royal Society Open Science*, vol. 6, no. 4, Article ID 181817, 2019.

[11] X. Li and Y. Chai, "Determination of pillar width to improve mining safety in a deep burst-prone coal mine," *Safety Science*, vol. 113, pp. 244–256, 2019.

[12] Q. Huang and J. Cao, "Research on coal pillar malposition distance based on coupling control of three-field in shallow buried closely spaced multi-seam mining, China," *Energies*, vol. 12, no. 3, p. 462, 2019.

[13] H. J. Luan, Y. J. Jiang, L. J. Zhou, and H. L. Lin, "Stability control and quick retaining technology of gob-side entry: a case study," *Advances in Civil Engineering*, vol. 2018, Article ID 7357320, 13 pages, 2018.

[14] M. Wang, J. Bai, W. Li, X. Wang, and S. Cao, "Failure mechanism and control of deep gob-side entry," *Arabian Journal of Geosciences*, vol. 8, no. 11, pp. 9117–9131, 2015.

[15] H. Su, J. Bai, S. Yan, Y. Chen, and Z. Zhang, "Study on gob-side entry retaining in fully-mechanized longwall with top-coal caving and its application," *International Journal of Mining Science and Technology*, vol. 25, no. 3, pp. 503–510, 2015.

[16] X. Z. Hua, S. Liu, Z. H. Liu, W. H. Zha, and Y. F. Li, "Research on strata pressure characteristic of gob-side entry driving in island mining face and its engineering application," *Chinese Journal of Rock Mechanics and Engineering*, vol. 30, no. 8, pp. 1646–1651, 2011.

[17] Y. Zhang, J. Tang, D. Xiao, L. Sun, and W. Zhang, "Spontaneous caving and gob-side entry retaining of thin seam with large inclined angle," *International Journal of Mining Science and Technology*, vol. 24, no. 4, pp. 441–445, 2014.

[18] P. Gong, Z. G. Ma, R. R. C. Zhang, X. Y. Ni, F. Liu, and Z. M. Huang, "Surrounding rock deformation mechanism and control technology for gob-side entry retaining with fully mechanized gangue backfilling mining: a case study," *Shock and Vibration*, vol. 2017, Article ID 6085941, 15 pages, 2017.

[19] S. Zhang, X. Wang, G. Fan, D. Zhang, and C. Jianbin, "Pillar size optimization design of isolated island panel gob-side entry driving in deep inclined coal seam-case study of Pingmei no. 6 coal seam," *Journal of Geophysics and Engineering*, vol. 15, no. 3, pp. 816–828, 2018.

[20] L. Deng, J. Lv, and Y. Chen, "Supporting a retained gob-side entry under soft and fractured rock: computer simulations and a practical example," *Geotechnical and Geological Engineering*, vol. 37, no. 3, pp. 2283–2292, 2019.

[21] X. M. Sun, L. Gan, Z. Chengwei et al., "Numerical investigation of gob-side entry retaining through precut overhanging hard roof to control rockburst," *Advances in Civil Engineering*, vol. 2018, Article ID 8685427, 10 pages, 2018.

[22] J. Yang, M. He, and C. Cao, "Design principles and key technologies of gob side entry retaining by roof pre-fracturing," *Tunnelling and Underground Space Technology*, vol. 90, pp. 309–318, 2019.

[23] X. Yang, E. Wang, X. Ma, G. Zhang, R. Huang, and H. Lou, "A case study on optimization and control techniques for entry stability in non-pillar longwall mining," *Energies*, vol. 12, no. 3, p. 391, 2019.

[24] M. Xingen, H. Manchao, W. Yajun, Z. Yong, Z. Jiabin, and L. Yuxing, "Study and application of roof cutting pressure releasing technology in retracement channel roof of halagou 12201 working face," *Mathematical Problems in Engineering*, vol. 2018, Article ID 6568983, 15 pages, 2018.

[25] Z. Tao, Z. Song, M. He, Z. Meng, and S. Pang, "Principles of the roof cut short-arm beam mining method (110 method) and its mining-induced stress distribution," *International Journal of Mining Science and Technology*, vol. 28, no. 3, pp. 391–396, 2018.

[26] Y. Wang, Y. Gao, E. Wang, M. He, and J. Yang, "Roof deformation characteristics and preventive techniques using a novel non-pillar mining method of gob-side entry retaining by roof cutting," *Energies*, vol. 11, no. 3, p. 627, 2018.

[27] Y. J. Wang, M. C. He, K. X. Zhang et al., "Strata behavior characteristics and control countermeasures for the gateroad surroundings in innovative non-pillar mining method with gateroad formed automatically," *Journal of Mining & Safety Engineering*, vol. 35, pp. 677–685, 2018.

[28] Q. Wang, M. He, J. Yang, H. Gao, B. Jiang, and H. Yu, "Study of a no-pillar mining technique with automatically formed gob-side entry retaining for longwall mining in coal mines," *International Journal of Rock Mechanics and Mining Sciences*, vol. 110, pp. 1–8, 2018.

[29] Y. F. Li and X. Z. Hua, "Mechanical analysis of stability of key blocks of overlying strata for gob-side entry retaining and calculating width of roadside backfill," *Rock and Soil Mechanics*, vol. 33, no. 4, pp. 1134–1140, 2012.

[30] M. G. Qian, P. W. Shi, and J. L. Xu, *Mine Stress and Ground Control*, China University of Mining and Technology Press, Xuzhou, China, 2010.

[31] Q. X. Huang, "Studies on load-transmitting factor of thick sandy soil layer on key roof stratum in shallow seam mining," *Chinese Journal of Geotechnical Engineering*, vol. 27, no. 6, pp. 672–676, 2005.

[32] C. J. Hou and N. J. Ma, "Stress in in-seam roadway side and limit equilibrium zone," *Journal of China Coal Society*, vol. 4, pp. 21–29, 1989.

[33] G. C. Zhang, Z. J. Wen, S. J. Liang, Y. L. Tan, L. Tian, and D. S. Zhao, "Ground response of a gob-side entry in a longwall panel extracting 17 m-thick coal seam: a case study," *Rock Mechanics and Rock Engineering*, pp. 1–20, 2019.

[34] Z. Li, J. Xu, J. Ju, W. Zhu, and J. Xu, "The effects of the rotational speed of voussoir beam structures formed by key strata on the ground pressure of stopes," *International Journal of Rock Mechanics and Mining Sciences*, vol. 108, pp. 67–79, 2018.

[35] C.-l. Han, N. Zhang, B.-y. Li, G.-y. Si, and X.-g. Zheng, "Pressure relief and structure stability mechanism of hard roof for gob-side entry retaining," *Journal of Central South University*, vol. 22, no. 11, pp. 4445–4455, 2015.

[36] J. Ning, J. Wang, X. Liu, K. Qian, and B. Sun, "Soft-strong supporting mechanism of gob-side entry retaining in deep coal seams threatened by rockburst," *International Journal of Mining Science and Technology*, vol. 24, no. 6, pp. 805–810, 2014.

[37] J. Chen, J. P. Du, W. S. Zhang, and J. X. Zhang, "An elastic base beam model of overlying strata movement during coal mining with gangue back-filling," *Journal of China University of Mining & Technology*, vol. 41, no. 1, pp. 14–19, 2012.

[38] Y. B. Gao, M. C. He, J. Yang, and X. G. Ma, "Experiment study of caving and distribution of gangues influenced by roof fracturing in pillarless mining with gob-side entry retaining," *Journal of China University of Mining & Technology*, vol. 47, no. 1, pp. 21–31, 2018.